COMMUNICATION

Check for updates

Efficient stacking of iso-butene in sulfonate functional metal–organic frameworks for efficient iso-butene/iso-butane separation†

Zhensong Qiu,‡[a] Jiyu Cui,‡[a] Dengzhuo Zhou,[a] Zhenglu Yang,[ab] Xiaofei Lu,[b] Xian Suo,[b] Anyun Zhang, [ID][a] Xili Cui, [ID][ab] Lifeng Yang*[ac] and Huabin Xing [ID]*[ab]

Separation of iso-butene and iso-butane is vital to producing high purity iso-butene feedstock, but is challenging because of their close molecular size and properties. Adsorptive separation using porous materials like metal organic frameworks (MOFs) is emerging as a potential energy-efficient alternative. But it's hindered by the lack of porous materials that exhibit satisfactory iso-butene/iso-butane separation performance. In this study, a novel sulfonate functionalized material, ZU-603, is reported to achieve the benchmark separation performance of iso-butene/iso-butane *via* exploiting the geometric difference of the carbon backbone between the planar iso-butene and tetrahedral iso-butane. Single-crystal analysis of ZU-603 loaded with iso-butene and simulation studies reveal that the sulfonate sites bound the iso-butene *via* $S^{\delta-}\cdots H^{\delta+}$=C interactions, meanwhile iso-butene molecules are efficiently stacked *via* π–π interactions within the confined space, realizing higher stacking efficiency of iso-butene than iso-butane. ZU-603 shows an exceptionally high iso-butene adsorption uptake of 2.30 mmol g^{-1} (298 K, 1 bar) and a record high iso-butene/iso-butane uptake ratio of 2.77 at 1 bar, outperforming previously reported benchmarking materials (1.2). Fixed-bed breakthrough experiments confirm the impressive iso-butene/iso-butane dynamic separation ability of ZU-603. The work provides a potential shape-recognition strategy in designing functional materials for the efficient separation of hydrocarbons with similar physicochemical properties.

[a] *Engineering Research Center of Functional Materials Intelligent Manufacturing of Zhejiang Province, College of Chemical and Biological Engineering, Zhejiang University, HangzhouZhejiang 310058, PR China. E-mail: lifeng_yang@zju.edu.cn, xinghb@zju.edu.cn*

[b] *ZJU-Hangzhou Global Scientific and Technological Innovation Center, Hangzhou 311215, China*

[c] *State Key Laboratory of Silicon Materials, School of Materials Science and Engineering, Zhejiang University, Hangzhou 310027, China*

† Electronic supplementary information (ESI) available: Additional figures, crystal information. See DOI: https://doi.org/10.1039/d5im00077g

‡ These authors contributed equally.

Keywords: Adsorptive separation; Hydrocarbon; Metal-organic frameworks; Iso-butene/iso-butane; Purification.

1 Introduction

Iso-butene (iso-C_4H_8) is an important feedstock in the petroleum industry, which could be utilized in producing butyl rubber, methyl methacrylate (MMA) and other high-performance materials.[1–4] One of the primary industrial sources of iso-C_4H_8 is the catalytic dehydrogenation of iso-butane (iso-C_4H_{10}), the product of which typically consists of approximately equal mole fractions of iso-C_4H_8 and iso-C_4H_{10} isomers due to the limited conversion rate.[5–7] To obtain high purity iso-C_4H_8 from the mixture, an industrial practice is to react the mixture with methanol to convert iso-C_4H_8 into methyl *tert*-butyl ether (MTBE).[8–10] Then MTBE is separated from iso-C_4H_{10} and cracked back into iso-C_4H_8 and methanol.[11] This complicated purification process may be simplified by the more convenient technology of adsorption separation.[12–14] The potential application of adsorption separation has been widely investigated in separating chemicals with similar physiochemical properties.[15–21] The key to adsorption separation is the design and application of high-performance porous materials. In recent years, metal organic frameworks (MOFs) with their extremely variable pore structures and highly tunable nature have shown promising application potential in the separation of hydrocarbon gas mixtures with very close physiochemical properties,[22–26] including ethane/ethylene,[27–31] ethylene/acetylene,[32–37] propane/propylene,[38–44] C6 isomers,[45–48] *etc.* HKUST-1 shows preferential adsorption of iso-C_4H_8 over iso-C_4H_{10} in the very low-pressure range of 0.5 kPa. However, it demonstrates negligible selectivity at higher pressures, limiting its separation performance.[49] Other than that, little attention has been paid to investigating the adsorption separation of iso-C_4H_8 and iso-C_4H_{10} using MOFs.

The properties of iso-C_4H_8 and iso-C_4H_{10} are very similar, where the most significant difference lies in the presence of a C=C double bond in the iso-C_4H_8 molecule. As a result, the 4 carbon atoms of iso-C_4H_8 are in the same plane while the 4 carbon atoms of the iso-C_4H_{10} molecule form a triangular pyramid. If this shape difference in the carbon backbone of the 2 isomers could be utilized to discriminate one another, the adsorption separation of iso-C_4H_8 and iso-C_4H_{10} could be achieved with high selectivity. Shape selective materials have been developed in the literature for the separation of butadiene,[50] xylene isomers,[51,52] etc. A feasible strategy is to construct pore cages with limited space and suitable shape to accommodate the desired molecule. The single pore cage of the material could simultaneously accommodate multiple target molecules with suitable molecular shape when the molecules are densely packed. But for the undesired molecules with inappropriate molecular shape, a single pore cage could hardly accommodate multiple molecules, realizing the preferential adsorption of the target molecule.
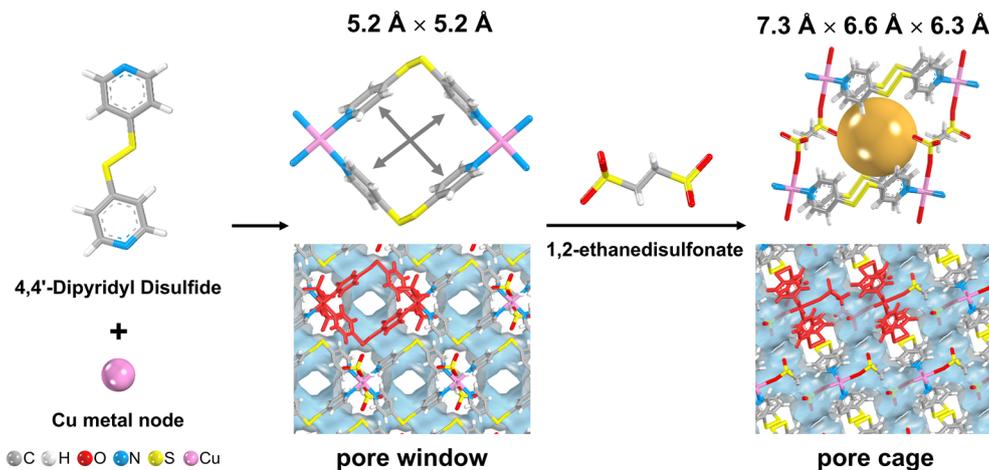
In this work, a shape-recognizing sulfonate functional material, ZU-603, was found to be capable of separating the iso-C_4H_8 and iso-C_4H_{10} mixture. Pure component adsorption isotherms show that ZU-603 exhibits higher adsorption affinity toward iso-C_4H_8 over iso-C_4H_{10} with an iso-C_4H_8/iso-C_4H_{10} uptake ratio of 2.77, superior to previously reported HKUST-1 (1.2).[49] Fixed bed breakthrough experiments further prove the separation performance of ZU-603. The structures of single crystals loaded with iso-C_4H_8 molecules were solved to unveil the adsorption behavior. Coupled with the DFT-D simulation, the separation mechanism was revealed.

2 Results and discussion

Mild conditions of ambient temperature and pressure are utilized for the synthesis of ZU-603, with methanol and water as solvents. The mild synthesis conditions enable ZU-603 to be further scaled-up. The Cu metal node is coordinated with the 4,4′-dipyridyl disulfide ligand to form the pore windows of ZU-603, with an opening of approximately 5.2 Å × 5.2 Å (Fig. 1), close to the molecular dimensions of iso-C_4H_8 and iso-C_4H_{10} (Fig. S1†). The sulfonate anion, 1,2-ethanedisulfonate, serves as the connecting unit of the pore windows, which further forms the pore cage (as illustrated by the orange sphere in Fig. 1) of ZU-603. It's revealed that the pore cages are connected to form a 2D layered structure (Fig. S2†). And then multiple 2D layered structures are stacked together to form the 3D structure of ZU-603, which endows it with the *sql* topology (Fig. S3†). The powder X-ray diffraction patterns of the synthesized samples match well with the simulated ones, confirming the high purity of the synthesized materials (Fig. 2f). Besides, the permanent porosity of ZU-603 is investigated *via* N_2 adsorption experiments at 77 K (Fig. S4†), which displays a Brunauer–Emmett–Teller (BET) surface area of 214 m^2 g^{-1} (Fig. S5†). Thermogravimetric analysis shows that ZU-603 is stable up to 240 °C (Fig. S6†). The SEM image of ZU-603 shows a flake-like morphology with a narrow size distribution in the range of 0.9–1.2 μm (Fig. S7†).

To explore the adsorptive properties of ZU-603 for iso-C_4H_8 and iso-C_4H_{10}, pure component adsorption–desorption isotherms are collected at 298 K and 313 K (Fig. 2a and b and S8†). It's displayed that ZU-603 shows higher adsorption affinity toward iso-C_4H_8 over iso-C_4H_{10} at both temperatures. At 298 K, ZU-603 exhibits a steep iso-C_4H_8 uptake at the pressure as low as 0.003 bar. The iso-C_4H_8 uptake is 2.30 mmol g^{-1} at 1 bar. For iso-C_4H_{10}, the uptake at 1 bar is 0.83 mmol g^{-1}. The iso-C_4H_8/iso-C_4H_{10} uptake at 1 bar is 2.77, higher than that of HKUST-1 (1.2).[49] Ideal adsorbed solution theory was applied to calculate the adsorption selectivity

5.2 Å × 5.2 Å   **7.3 Å × 6.6 Å × 6.3 Å**

4,4'-Dipyridyl Disulfide

+

Cu metal node

C   H   O   N   S   Cu

1,2-ethanedisulfonate

pore window   **pore cage**

Fig. 1   The building blocks of the pore window of ZU-603 and the illustration of the pore window. The sulfonate anion is used to connect the pore window to construct the 3D framework of ZU-603, and the illustration of the pore cage is derived from the assembly of the pore window and the sulfonate anion. The van der Waals radius of hydrogen (1.1 Å) is deducted when taking the measurements (color code: silver, C; white, H; red, O; blue, N; yellow, S; pink, Cu; orange, illustration of the space within the expanded pore cage. The components that build a single contracted pore window and a single expanded pore cage are highlighted in red for clarity).
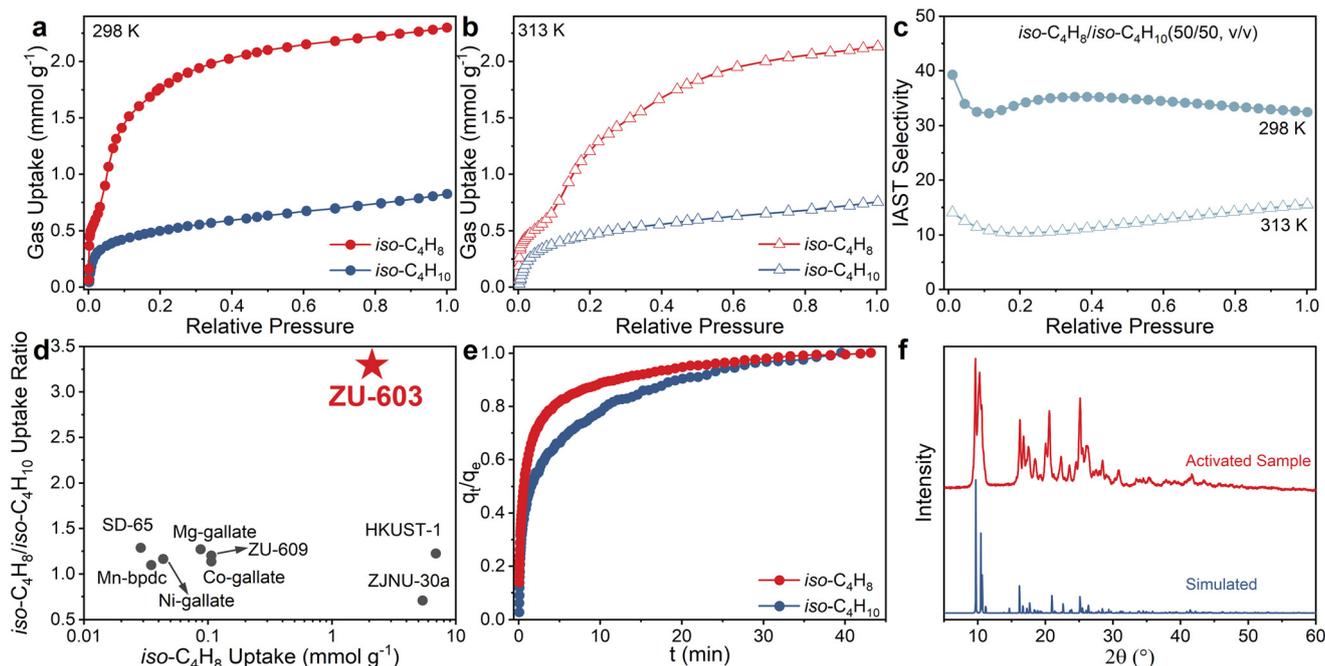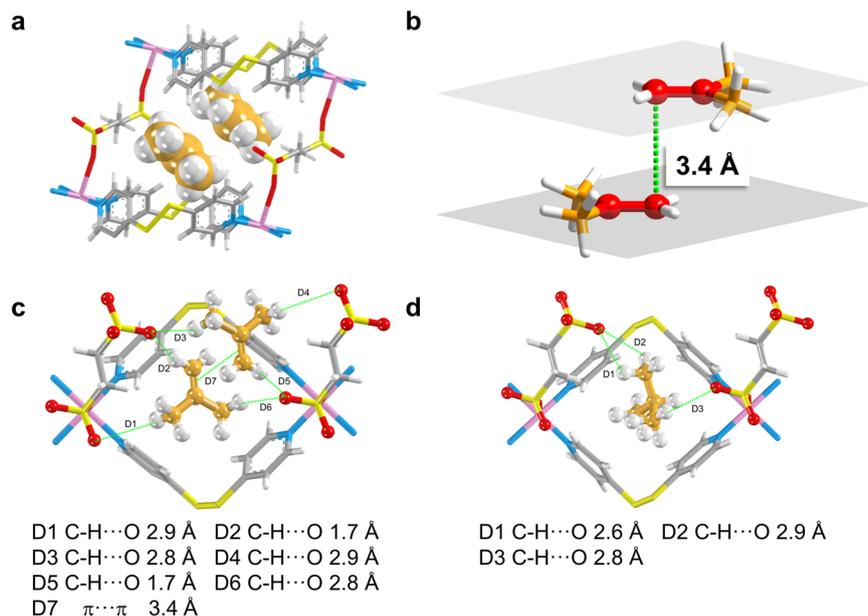
Fig. 2 Pure component adsorption isotherms of iso-C_4H_8 and iso-C_4H_{10} on ZU-603 at (a) 298 K and (b) 313 K; (c) iso-C_4H_8/iso-C_4H_{10} (50/50) IAST selectivity of ZU-603 calculated in the pressure range of 0–1 bar at 298 K and 313 K; (d) comparison of uptake ratio of iso-C_4H_8 (0.5 bar)/iso-C_4H_{10} (0.5 bar) and iso-C_4H_8 (0.5 bar) uptake of ZU-603 against other reported materials; (e) time dependent adsorption profiles of iso-C_4H_8 and iso-C_4H_{10} at 298 K and 0.6 bar; (f) powder X-ray diffraction patterns (PXRD) of the activated sample and pattern simulated using the crystal structure of ZU-603.

(IAST selectivity). At infinity dilution, the IAST selectivity is 39 at 298 K and 14 at 313 K (Fig. 2c and S9 and S10†). It's noted that ZU-603 not only possesses a very high iso-C_4H_8 uptake of 2.10 mmol g^{-1} at 0.5 bar, but also shows the highest iso-C_4H_8/iso-C_4H_{10} uptake ratio of 3.33 at 0.5 bar compared with other reported materials (Fig. 2d): SD-65 (1.29),[53] Mg-gallate (1.27),[54] ZU-609 (1.20),[55] and HKUST-1 (1.23).[49] The time dependent adsorption profiles of both isomers were further measured to investigate the diffusion rate of iso-C_4H_8 and iso-C_4H_{10} within the pores of ZU-603 (Fig. 2e). The diffusion time constants of iso-C_4H_8 and iso-C_4H_{10} were calculated using the micropore diffusion model, which are 7.42×10^{-4} s^{-1} and 6.43×10^{-4} s^{-1} for iso-C_4H_8 and iso-C_4H_{10}, respectively (Fig. S11 and S12†). The result indicates that both isomers show a close diffusion rate within the pores of ZU-603.

Grand Canonical Monte Carlo (GCMC) simulation was used to elucidate the preferential adsorption of iso-C_4H_8 over iso-C_4H_{10} at a fixed pressure of 1 atm. Snapshots at different steps are taken to understand the adsorption process (Fig. S13 and S14†). The two images compare the adsorption behaviour of iso-C_4H_8 and iso-C_4H_{10} in ZU-603 at 1 bar. Iso-C_4H_8 shows significantly higher uptake, with dense and progressive filling of the framework cavities from panel (1) to (10), while iso-C_4H_{10} adsorption remains sparse even at saturation. This contrast highlights ZU-603's selective adsorption driven by stronger interactions with the unsaturated iso-C_4H_8 likely due to π-complexation or better shape compatibility. In addition, the low energy snapshot

of iso-C_4H_8 also shows a higher packing density than that of iso-C_4H_{10} (Fig. S15†). The average loading of iso-C_4H_8 is 0.77 molecules per unit cell and iso-C_4H_{10} is 0.21 molecules per unit cell, yielding an uptake ratio of 3.66 at 1 bar, which is very similar to the experimental result of 2.77. To further unveil the higher adsorption uptake of iso-C_4H_8 over iso-C_4H_{10}, the structures of the single crystals loaded with iso-C_4H_8 were successfully obtained. It's found that 2 iso-C_4H_8 molecules could be simultaneously adsorbed within the same pore cage of ZU-603 (Fig. 3a). This allows the maximized occupation of the pore space. Further investigation into the packing diagram of the 2 iso-C_4H_8 molecules adsorbed reveals the reason behind such a phenomenon. Due to the double bond of iso-C_4H_8 molecules, the 4 carbon atoms of iso-C_4H_8 are distributed in the same plane, which could be utilized to pack two iso-C_4H_8 molecules in a space efficient way. In detail, the 2 iso-C_4H_8 molecules are stacked in a confined pore cage of ZU-603 in a way that the aforementioned planes within each iso-C_4H_8 run parallel to each other, with a distance of 3.4 Å between the two planes (Fig. 3b). This facilitates the space-efficient packing of iso-C_4H_8 in the limited space of the pore cages within ZU-603, which could not be achieved by iso-C_4H_{10}. The O atoms of the sulfonate anions are the primary binding site of iso-C_4H_8, with the C–H⋯O hydrogen bond in the range of 1.7–2.9 Å (Fig. 3c). DFT-D calculation was applied to calculate the specific binding sites of iso-C_4H_{10} within ZU-603. The result show that like iso-C_4H_8, O atoms of the sulfonate anions are also the

© 2025 The Author(s). Co-published by the Institute of Process Engineering, Chinese Academy of Sciences and the Royal Society of Chemistry

Ind. Chem. Mater., 2025, **3**, 535–542 | **537**

3.4 Å

D1 C–H⋯O 2.9 Å   D2 C–H⋯O 1.7 Å
D3 C–H⋯O 2.8 Å   D4 C–H⋯O 2.9 Å
D5 C–H⋯O 1.7 Å   D6 C–H⋯O 2.8 Å
D7 π⋯π 3.4 Å

D1 C–H⋯O 2.6 Å   D2 C–H⋯O 2.9 Å
D3 C–H⋯O 2.8 Å

Fig. 3 (a) 2 iso-C_4H_8 molecules adsorbed in one pore cage of ZU-603 as revealed by single crystal analysis; (b) the packing diagram of 2 iso-C_4H_8 molecules adsorbed within one pore cage of ZU-603 as revealed by single crystal analysis; (c) the specific binding sites of iso-C_4H_8 on ZU-603 as revealed by single crystal experiments; (d) the specific binding sites of iso-C_4H_{10} on ZU-603 as revealed by DFT-D calculations (color code: silver, C; white, H; red, O; blue, N; yellow, S; pink, Cu; orange, C of the adsorbed molecules).

main binding sites of iso-C_4H_{10}, where the C–H⋯O hydrogen bond is in the range of 2.6–2.9 Å (Fig. 3d).

A fixed bed breakthrough experiment with a gas mixture of iso-C_4H_8/iso-C_4H_{10} (50/50, v/v) was carried out to investigate the dynamic separation performance of ZU-603. The results show that ZU-603 could selectively adsorb iso-C_4H_8 in the binary mixture with a breakthrough sequence of iso-C_4H_8 < iso-C_4H_{10}. After the introduction of the gas mixture, both isomers were adsorbed within the column packed with ZU-603 until 23.5 min, where iso-C_4H_{10} first elutes. Iso-C_4H_8 did not breakthrough until 50 min, with an effective dynamic adsorption capacity of 1.06 mmol g^{-1}. The results show a good dynamic separation performance of ZU-603 for the binary mixture (Fig. 4a). Cycling adsorption experiments of pure component iso-C_4H_8 show no obvious gas uptake loss

after 5 cycles, exhibiting the good cycling capacity of ZU-603 (Fig. 4b).

3 Conclusions

In summary, a novel sulfonate functionalized ultramicroporous material, ZU-603, was designed and it exhibits an excellent iso-C_4H_8/iso-C_4H_{10} separation performance because of its selective shape-recognizing ability toward iso-C_4H_8 molecules over iso-C_4H_{10}. Through exploiting the C=C double bond and the planar configuration of iso-C_4H_8, ZU-603 with suitable pore size and distributed sulfonate functional sites induces the effective packing of 2 iso-C_4H_8 molecules within the limited volume of 1 pore cage of the material via $S^{\delta-}$⋯$H^{\delta+}$=C interactions and π–π guest–guest interactions. This work not only provides an
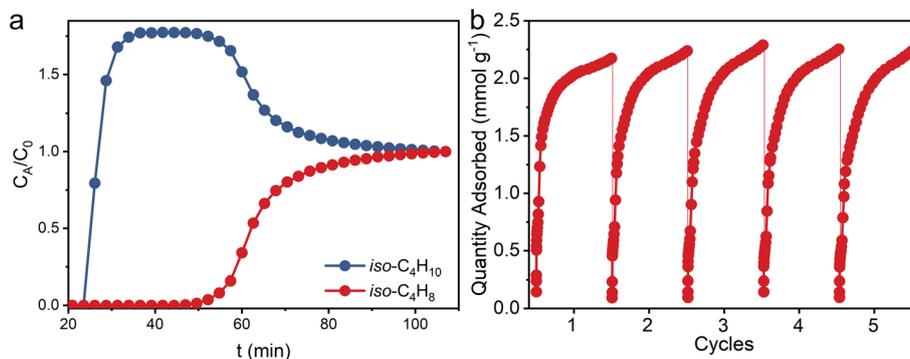
Fig. 4 (a) Breakthrough experiment on ZU-603 using a gas mixture of iso-C_4H_8/iso-C_4H_{10} (50/50, v/v) with a mix gas flow rate of 0.8 mL min^{-1} at 298 K and (b) cycling adsorption tests of iso-C_4H_8 on ZU-603 at 298 K.

important case of iso-C_4H_8/iso-C_4H_{10} porous materials with both high capacity and selectivity, but also demonstrates the shape-recognizing strategy in the separation of C4 hydrocarbons, which may also be applied in designing high-performance materials for other challenging separations.

4 Experimental section

Materials

All chemicals were used as received without further purification. 4,4′-Dipyridyl disulfide (>97%) was purchased from TCI Chemicals, and 1,2-ethanedisulfonate disodium salt (98%) was purchased from Energy Chemical. $Cu(NO_3)_2 \cdot 3H_2O$ (AR) and methanol (AR) were purchased from Sinopharm Chemical Reagent Co., Ltd.

Synthesis of ZU-603 (powder)

4,4′-Dipyridyl disulfide (1 mmol, 0.220 g) is dissolved in 20 mL anhydrous methanol, yielding the ligand solution. $Cu(NO_3)_2 \cdot 3H_2O$ (0.5 mmol, 0.121 g) and 1,2-ethanedisulfonate disodium salt (0.5 mmol, 0.117 g) are dissolved in 3 mL deionized water, after which 10 mL anhydrous methanol is added to the salt solution. The salt solution is then slowly added to the ligand solution under constant stirring. The composite is then stirred for 24 h at 25 °C. The purple product is obtained by filtration and purified by washing with 250 mL anhydrous methanol. The product is then soaked in anhydrous methanol for 3 days.

Synthesis of ZU-603 (single crystal)

$Cu(NO_3)_2 \cdot 3H_2O$ (0.02 g) and 1,2-ethanedisulfonate disodium salt (0.02 g) are dissolved in 20 mL deionized water. 4,4′-Dipyridyl disulfide (0.02 g) is dissolved in 20 mL methanol. Then the methanol solution is carefully layered onto the water solution at ambient temperature. The single crystals of ZU-603 are obtained after two weeks.

Single crystal X-ray crystallography

The crystal structures of ZU-603 and iso-C_4H_8 loaded ZU-603 are determined by single crystal X-ray diffraction experiments. The X-ray diffraction experiments are conducted using a Bruker D8 Venture diffractometer equipped with a PHOTONII/CMOS detector (GaKα, λ = 1.34139 Å). Data collection is performed using APEX3, and the dataset of each sample is integrated and reduced using SaintPlus 6.01. The space group of the material is determined using XPREP in APEX3. Structure solutions and refinements are carried out with SHELXS-201 and SHELXL-2018 with APEX3 for the samples described above. The CIF file of ZU-603 has been deposited at CCDC (2453159).

Thermogravimetric analysis (TGA)

The thermal gravimetric analysis is performed on a TGA Q500 V20.13 Build 39. Experiments are carried out using a platinum pan under nitrogen atmosphere which is conducted by a flow rate of 60 mL min^{-1} nitrogen gas. The data are collected in the temperature range of 55 °C to 900 °C with a ramp of 10 °C min^{-1}.

Scanning electron microscopy (SEM)

The morphology of ZU-603 was characterized using a Hitachi SU-8010 scanning electron microscope.

N$_2$ adsorption measurements

N$_2$ adsorption and desorption isotherms on activated materials are measured on a Micromeritics ASAP 2460 surface area analyzer at 77 K.

C4 gas equilibrium adsorption measurements

Iso-C_4H_8 and iso-C_4H_{10} isotherms are collected on a Micromeritics ASAP 2050 surface area analyzer at 298 K.

Kinetic adsorption measurement

The time-dependent adsorption profiles of different C4 isomers on ZU-603 are measured using a BEL-SORP-max II at 0.6 bar and 298 K or 313 K. For the experiments at the specified pressure, a fixed amount of target gas is introduced into the sample chamber, and then the equipment monitors the pressure in the chamber until it becomes stable.

Breakthrough experiments

The fixed-bed breakthrough experiments and cycling tests are carried out on dynamic gas breakthrough equipment. All experiments are conducted using stainless-steel columns with an inner diameter of 4.6 mm and a length of 10 cm. The ZU-603 sample packed in the column is 0.8409 g. The packing density is calculated to be 0.506 g cm^{-3}, which remained the same after constant N$_2$ purging at 20 mL min^{-1} for 24 hours. The gas mixture consists of 1 : 1 mole ratio iso-C_4H_8, and iso-C_4H_{10}. The column packed with porous materials are regenerated by purging dry N$_2$ with a flow rate of 20 mL min^{-1} at 100 °C overnight.

Grand Canonical Monte Carlo (GCMC) simulation

The gradual packing of iso-C_4H_8 and iso-C_4H_{10} was determined through GCMC simulations in the sorption module. The framework of ZU-603 was first optimized by DFT-D calculations, and considered to be rigid during the simulation. The charges for atoms of ZU-603 were derived from Qeq method and Qeq_charged 1.1 parameters. The simulations adopted the task of fixed pressure at 100 kPa, the Metropolis method in the sorption module, the universal force field (UFF) for ZU-603, and the configurational bias method in the sorption module. The interaction energy between the adsorbed molecules and the framework was computed through the Coulomb and Lennard-Jones 6–12 (LJ) potentials. The cutoff radius was chosen as 18.5 Å for LJ potential and the long range electrostatic interactions were handled using the Ewald summation method. The loading

steps and the equilibration steps were 1×10^7; the production steps were 1×10^7.

Dispersion-corrected density functional theory (DFT-D) calculations

The Quantum-Espresso package is applied for dispersion-corrected density-functional theory (DFT-D) calculations. The van der Waals interactions are accounted for by the addition of semi-empirical dispersive forces to conventional DFT-D. Vanderbilt-type ultrasoft pseudopotentials and generalized gradient approximation (GGA) with Perdew–Burk–Ernzerhof (PBE) exchange corrections are utilized. A cutoff energy of 544 eV and a $3 \times 3 \times 3$ k-point mesh (generated using the Monkhorst–Pack scheme) are enough for the total energy to converge within 0.01 meV per atom. The structure of ZU-603 is first optimized and the results are a good match for the experimentally determined crystal structure of the material. Iso-C_4H_{10} molecules are then introduced to various locations of the pore channels, followed by a full structural relaxation.

Calculation of ideal adsorbed solution theory (IAST) selectivity

The software IAST++ is used for the calculation of IAST selectivity. Using the Dual-Site Langmuir–Freundlich (DSLF) model, the adsorption isotherms of iso-C_4H_8 and iso-C_4H_{10} on ZU-603 at 298 K are fitted. The fitted model parameters are input into the software to calculate the IAST selectivity at 298 K for an iso-C_4H_8/iso-C_4H_{10} mixture with a 0.5/0.5 composition ratio. The employed model equation is shown in eqn (1):

$$n(P) = q_1 \frac{(k_1 P)^{n_1}}{1 + (k_1 P)^{n_1}} + q_2 \frac{(k_2 P)^{n_2}}{1 + (k_2 P)^{n_2}} \quad (1)$$

where $n(P)$ is the adsorption amount at pressure P; P is the equilibrium pressure of the gas phase; q_1, q_2, k_1, k_2, n_1, n_2 are the fitted constants.

The equation for IAST selectivity is given by eqn (2):

$$S_{ads} = \frac{q_1/q_2}{p_1/p_2} \quad (2)$$

where q_1 and q_2 are the molar amounts of the two components adsorbed, and p_1 and p_2 are the partial pressures of the two components in the gas phase.

Calculation of diffusion time constants

The time dependent adsorption profiles of iso-C_4H_8 and iso-C_4H_{10} on ZU-603 are fitted using the micropore diffusion model,[56,57] from which the diffusion time constant D_c/r_c^2 of the gas was obtained. The specific equation is as follows:

$$\frac{q_t}{q_e} \approx \frac{6}{\sqrt{r_c}} \sqrt{\frac{D_c t}{\pi}} (q_t/q_e < 0.3) \quad (3)$$

where q_t is the amount of gas adsorbed at time t; q_e is the equilibrium adsorption capacity; q_t/q_e is obtained from the instrument; D_c is the diffusion coefficient of a specific gas component in ZU-603; r_c is the equivalent radius of the adsorbent particles.

Data availability

The data supporting this article have been included as part of the ESI.†

Author contributions

H. X. and L. Y. initiated and supervised the research. Z. Q., J. C., and D. Z. performed material synthesis and data collection. Z. Y. performed DFT-D calculation. Z. Q., J. C., L. Y., X. L., X. S., and X. C. engaged in data analysis. A. Z., X. S., X. C., and X. L., engaged in discussion and draft editing. Z. Q., J. C., L. Y. and H. X. engaged in manuscript preparation and revision.

Conflicts of interest

The authors declare no conflict of interest.

References

1 P. Yao, H. Wu, N. Ning, L. Zhang, H. Tian, Y. Wu, G. Hu, T. W. Chan and M. Tian, Properties and unique morphological evolution of dynamically vulcanized bromo-isobutylene-isoprene rubber/polypropylene thermoplastic elastomer, *RSC Adv.*, 2016, **6**, 11151–11160.

2 K. Gong, H. Tian, H. Liu, X. Liu, G.-H. Hu, B. Yu, N. Ning, M. Tian and L. Zhang, Grafting of isobutylene–isoprene rubber with glycidyl methacrylate and its reactive compatibilization effect on isobutylene–isoprene rubber/polyamides 12 blends, *Ind. Eng. Chem. Res.*, 2021, **60**, 16258–16266.

3 M. J. D. Mahboub, J.-L. Dubois, F. Cavani, M. Rostamizadeh and G. S. Patience, Catalysis for the synthesis of methacrylic acid and methyl methacrylate, *Chem. Soc. Rev.*, 2018, **47**, 7703–7738.

4 W. E. Luttrell, Isobutylene, *J. Chem. Health Saf.*, 2013, **20**, 35–37.

5 U. Rodemerck, E. V. Kondratenko, T. Otroshchenko and D. Linke, Unexpectedly high activity of bare alumina for non-oxidative isobutane dehydrogenation, *Chem. Commun.*, 2016, **52**, 12222–12225.

6 G. Wang, C. Li and H. Shan, Highly efficient metal sulfide catalysts for selective dehydrogenation of isobutane to isobutene, *ACS Catal.*, 2014, **4**, 1139–1143.

7   E. Cheng, L. McCullough, H. Noh, O. Farha, J. Hupp and J. Notestein, Isobutane dehydrogenation over bulk and supported molybdenum sulfide catalysts, *Ind. Eng. Chem. Res.*, 2019, **59**, 1113–1122.

8   F. Collignon, R. Loenders, J. Martens, P. Jacobs and G. Poncelet, Liquid phase synthesis of MTBE from methanol and isobutene over acid zeolites and amberlyst-15, *J. Catal.*, 1999, **182**, 302–312.

9   P. Chu and G. H. Kuhl, Preparation of methyl tert-butyl ether (MTBE) over zeolite catalysts, *Ind. Eng. Chem. Res.*, 1987, **26**, 365–369.

10   I. Stepchuk, M. Pérez-Fortes and A. Ramírez, Assessing impacts of deploying bio-based isobutene for MTBE production in an existing petrochemical cluster, *J. Cleaner Prod.*, 2025, 145114.

11   F. Lombardi and A. Compagnone, MTBE catalytic cracking for the production of high purity isobutene, *Master's thesis*, Politecnico di milano, 2019.

12   X. Peng, W. Wang, R. Xue and Z. Shen, Adsorption separation of CH_4/CO_2 on mesocarbon microbeads: Experiment and modeling, *AIChE J.*, 2006, **52**, 994–1003.

13   J.-X. Li, Y.-J. Zhao, Y.-F. Yu, Q.-Q. Huang, S.-C. Qi, X.-Q. Liu and L.-B. Sun, The selective adsorption of anionic dyes over 3D printing composite sorbents of aerogel and porous carbon, *Sep. Purif. Technol.*, 2025, **360**, 130945.

14   H. Zhang, K. Zhao, W. Guo, K. Liang, J. Li, X. Li, Q. Deng, X. Xu, H. Chao, H. Xi and C. Duan, Room-temperature rapid synthesis of hierarchically porous ZIF-93 for effective adsorption of volatile organic compounds, *Ind. Chem. Mater.*, 2025, **3**, 109–121.

15   Z. R. Herm, E. D. Bloch and J. R. Long, Hydrocarbon separations in metal–organic frameworks, *Chem. Mater.*, 2014, **26**, 323–338.

16   J.-W. Cao, T. Zhang, Y.-Q. Liu, Y. Wang, F.-P. Pan, J. Chen and K.-J. Chen, Precise C_2H_2 adsorption affinity modulation by nitrogen functionalization in isostructural coordination networks, *Small*, 2025, **21**, 2501924.

17   R. Yang, Y. Wang, J.-W. Cao, Z.-M. Ye, T. Pham, K. A. Forrest, R. Krishna, H. Chen, L. Li, B.-K. Ling, T. Zhang, T. Gao, X. Jiang, X.-O. Xu, Q.-H. Ye and K.-J. Chen, Hydrogen bond unlocking-driven pore structure control for shifting multi-component gas separation function, *Nat. Commun.*, 2024, **15**, 804.

18   Y. Jiang, T. Yang, X.-Q. Liu, P. Cui and L.-B. Sun, A metal–organic cage with light-switchable motifs for controllable CO_2 adsorption, *J. Mater. Chem. A*, 2024, **12**, 892–898.

19   Z. Xu, S. Chen, B. Yang, H. Zhou, L. Wang, B. E. Keshta, W. Zhu and Y. Zhang, Breakthrough developments in Metal-organic frameworks (MOFs) for efficient C4 hydrocarbon separation, *Chem. Eng. J.*, 2025, **508**, 160992.

20   S. Luo, T. Han, C. Wang, Y. Sun, H. Zhang, R. Guo and S. Zhang, Hierarchically microporous membranes for highly energy-efficient gas separations, *Ind. Chem. Mater.*, 2023, **1**, 376–387.

21   H. Yang, N. U. Afsar, Q. Chen, X. Ge, X. Li, L. Ge and T. Xu, Poly(alkyl-biphenyl pyridinium) anion exchange membranes with a hydrophobic side chain for mono−/divalent anion separation, *Ind. Chem. Mater.*, 2023, **1**, 129–139.

22   L. Yang, P. Zhang, J. Cui, X. Cui and H. Xing, The chemistry of metal–organic frameworks for multicomponent gas separation, *Angew. Chem.*, 2024, **136**, e202414503.

23   L. Yang, S. Qian, X. Wang, X. Cui, B. Chen and H. Xing, Energy-efficient separation alternatives: Metal–organic frameworks and membranes for hydrocarbon separation, *Chem. Soc. Rev.*, 2020, **49**, 5359–5406.

24   J.-R. Li, R. J. Kuppler and H.-C. Zhou, Selective gas adsorption and separation in metal–organic frameworks, *Chem. Soc. Rev.*, 2009, **38**, 1477–1504.

25   J.-J. Li, S.-Y. Liu, G. Liu, Y.-G. Liu, G.-Z. Wu, H.-D. Li, R. Krishna, X.-Q. Liu and L.-B. Sun, A robust perylene diimide-based zirconium metal–organic framework for preferential adsorption of ethane over ethylene, *Sep. Purif. Technol.*, 2023, **320**, 124109.

26   S. Du, X. Wang, J. Huang, K. Kent, B. Huang, I. Karam, Z. Li and J. Xiao, Ultramicroporous carbons featuring sub-Ångstrom tunable apertures for the selective separation of light hydrocarbon, *AIChE J.*, 2021, **67**, e17285.

27   L. Li, R.-B. Lin, R. Krishna, H. Li, S. Xiang, H. Wu, J. Li, W. Zhou and B. Chen, Ethane/ethylene separation in a metal-organic framework with iron-peroxo sites, *Science*, 2018, **362**, 443–446.

28   Y. Ma, C. Yu, L. Yang, R. You, Y. Bo, Q. Gong, H. Xing and X. Cui, Boosting kinetic separation of ethylene and ethane on microporous materials via crystal size control, *Chin. J. Chem. Eng.*, 2024, **65**, 85–91.

29   H. Yang, Y. Wang, R. Krishna, X. Jia, Y. Wang, A. N. Hong, C. Dang, H. E. Castillo, X. Bu and P. Feng, Pore-space-partition-enabled exceptional ethane uptake and ethane-selective ethane–ethylene separation, *J. Am. Chem. Soc.*, 2020, **142**, 2222–2227.

30   S.-M. Wang, H.-R. Liu, S.-T. Zheng, H.-L. Lan, Q.-Y. Yang and Y.-Z. Zheng, Control of pore structure by the solvent effect for efficient ethane/ethylene separation, *Sep. Purif. Technol.*, 2023, **304**, 122378.

31   Y. Peng, H. Xiong, P. Zhang, Z. Zhao, X. Liu, S. Tang, Y. Liu, Z. Zhu, W. Zhou, Z. Deng, J. Liu, Y. Zhong, Z. Wu, J. Chen, Z. Zhou, S. Chen, S. Deng and J. Wang, Interaction-selective molecular sieving adsorbent for direct separation of ethylene from senary C2-C4 olefin/paraffin mixture, *Nat. Commun.*, 2024, **15**, 625.

32   X. Cui, K. Chen, H. Xing, Q. Yang, R. Krishna, Z. Bao, H. Wu, W. Zhou, X. Dong and Y. Han, Pore chemistry and size control in hybrid porous materials for acetylene capture from ethylene, *Science*, 2016, **353**, 141–144.

33   Y.-Y. Xiong, H. Chen, C.-X. Chen, B. Lan, T. Pham, K. A. Forrest, Z.-W. Wei, M. Pan and C.-Y. Su, Enhancing acetylene/ethylene separation through cation exchange in an anion-pillared hybrid ultramicroporous MOF, *Ind. Eng. Chem. Res.*, 2024, **63**, 13826–13833.

34   Q.-L. Qian, X.-W. Gu, J. Pei, H.-M. Wen, H. Wu, W. Zhou, B. Li and G. Qian, A novel anion-pillared metal–organic framework for highly efficient separation of acetylene from

© 2025 The Author(s). Co-published by the Institute of Process Engineering, Chinese Academy of Sciences and the Royal Society of Chemistry

Ind. Chem. Mater., 2025, **3**, 535–542 | **541**

ethylene and carbon dioxide, *J. Mater. Chem. A*, 2021, **9**, 9248–9255.

35 P. Wang, S. Shang, H. Xiong, X. Liu, J. Liu, H. Shuai, L. Wang, Z. Zhu, Z. Zhao, Y. Peng, J. Chen, S. Chen, Z. Zhou and J. Wang, Engineering the pore size of interpenetrated metal–organic frameworks for molecular sieving separation of C_2H_2/C_2H_4, *J. Mater. Chem. A*, 2025, **13**, 1915–1922.

36 Y. Jiang, L. Wang, G. Xing, C. Liu, G. Xiong, D. Sun, J. Hu, W. Zhu, Z. Gu, B. Chen, T. Ben and Y. Zhang, Optimizing charge separated synergistic binding sites in self-Healing crystalline porous organic salts for benchmark trace alkyne/alkene separation, *Angew. Chem., Int. Ed.*, 2025, **64**, e202507442.

37 Y. Zhang, W. Sun, B. Luan, J. Li, D. Luo, Y. Jiang, L. Wang and B. Chen, Topological design of unprecedented metal-organic frameworks featuring multiple anion functionalities and hierarchical porosity for benchmark acetylene separation, *Angew. Chem.*, 2023, **62**, e202309925.

38 J. Cui, Z. Zhang, L. Yang, J. Hu, A. Jin, Z. Yang, Y. Zhao, B. Meng, Y. Zhou and J. Wang, A molecular sieve with ultrafast adsorption kinetics for propylene separation, *Science*, 2024, **383**, 179–183.

39 A. Cadiau, K. Adil, P. Bhatt, Y. Belmabkhout and M. Eddaoudi, A metal-organic framework–based splitter for separating propylene from propane, *Science*, 2016, **353**, 137–140.

40 R. A. Klein, L. W. Bingel, A. Halder, M. Carter, B. A. Trump, E. D. Bloch, W. Zhou, K. S. Walton, C. M. Brown and C. M. McGuirk, Adaptive pore opening to form tailored adsorption sites in a cooperatively flexible framework enables record inverse propane/propylene separation, *J. Am. Chem. Soc.*, 2023, **145**, 21955–21965.

41 Y. Zhong, Z.-M. Ye, F. Sha, H. Xie, X. Wang, C. Zhang, D. Lv, Y. Chen, Z. Li and O. K. Farha, Reduced-symmetry ligand constructed Y-Based metal–organic framework for Inverse propane/propylene separation, *ACS Mater. Lett.*, 2024, **6**, 5348–5353.

42 Z. Deng, L. Yang, H. Xiong, J. Liu, X. Liu, Z. Zhou, S. Chen, Y. Wang, H. Wang, J. Chen, S. Deng, B. Chen and J. Wang, Green and scalable preparation of an isomeric CALF-20 adsorbent with tailored pore size for molecular sieving of propylene from propane, *Small Methods*, 2025, **9**, 2400838.

43 S. Du, J. Huang, M. R. Ryder, L. L. Daemen, C. Yang, H. Zhang, P. Yin, Y. Lai, J. Xiao, S. Dai and B. Chen, Probing sub-5 Ångstrom micropores in carbon for precise light olefin/paraffin separation, *Nat. Commun.*, 2023, **14**, 1197.

44 S. Du, B. Huang, L. Zhu, Y. Wu, J. Huang, Z. Li, H. Yu and J. Xiao, Optimizing gas transport for C_3H_6/C_3H_8 size sieving separation via fine pore engineering of carbon microspheres, *Carbon*, 2023, **215**, 118451.

45 L. Li, Z. Yang, Q. Wang, L. Yang, X. Suo, X. Cui and H. Xing, Efficient separation of dibranched hexane from its linear and monobranched isomers via the synergistic molecular sieving and pore shape-matching strategy, *Small*, 2025, **21**, 2412724.

46 Q. Wang, L. Yang, T. Ke, J. Hu, X. Suo, X. Cui and H. Xing, Selective sorting of hexane isomers by anion-functionalized metal-organic frameworks with optimal energy regulation, *Nat. Commun.*, 2024, **15**, 2620.

47 E. Velasco, S. Xian, H. Wang, S. J. Teat, D. H. Olson, K. Tan, S. Ullah, T. M. Osborn Popp, A. D. Bernstein and K. A. Oyekan, Flexible Zn-MOF with rare underlying scu topology for effective separation of C6 alkane isomers, *ACS Appl. Mater. Interfaces*, 2021, **13**, 51997–52005.

48 B. Lal, K. B. Idrees, H. Xie, C. S. Smoljan, S. Shafaie, T. Islamoglu and O. K. Farha, Pore aperture control toward size-exclusion-based hydrocarbon separations, *Angew. Chem., Int. Ed.*, 2023, **135**, e202219053.

49 M. Hartmann, S. Kunz, D. Himsl, O. Tangermann, S. Ernst and A. Wagener, Adsorptive separation of isobutene and isobutane on $Cu_3 (BTC)_2$, *Langmuir*, 2008, **24**, 8634–8642.

50 P.-Q. Liao, N.-Y. Huang, W.-X. Zhang, J.-P. Zhang and X.-M. Chen, Controlling guest conformation for efficient purification of butadiene, *Science*, 2017, **356**, 1193–1196.

51 Q. Wang, Y. Li, Z. Qiu, D. Zhou, L. Yang, X. Suo, X. Cui and H. Xing, Highly efficient separation of intermediate-size m-xylene from xylenes via a length-matched metal–organic framework with optimal oxygen sites distribution, *Angew. Chem., Int. Ed.*, 2024, **136**, e202408817.

52 Y. Li, J. Cui, Q. Wang, L. Yang, L. Chen, H. Xing and X. Cui, Responsive shape recognition of styrene over ethylbenzene with excellent selectivity and capacity in a hybrid porous material, *Chem. Eng. J.*, 2023, **453**, 139756.

53 K. Kishida, Y. Okumura, Y. Watanabe, M. Mukoyoshi, S. Bracco, A. Comotti, P. Sozzani, S. Horike and S. Kitagawa, Recognition of 1, 3-butadiene by a porous coordination polymer, *Angew. Chem., Int. Ed.*, 2016, **55**, 13784–13788.

54 J. Chen, J. Wang, L. Guo, L. Li, Q. Yang, Z. Zhang, Y. Yang, Z. Bao and Q. Ren, Adsorptive Separation of Geometric Isomers of 2-Butene on Gallate-Based Metal–Organic Frameworks, *ACS Appl. Mater. Interfaces*, 2020, **12**, 9609–9616.

55 J. Cui, Z. Qiu, Z. Yang, A. Jin, X. Cui, L. Yang and H. Xing, One-step butadiene purification in a sulfonate-functionalized metal–organic framework through synergistic separation mechanism, *Angew. Chem., Int. Ed.*, 2024, **63**, e202403345.

56 N. S. Wilkins, J. A. Sawada and A. Rajendran, Diffusion of CH_4 and N_2 in Barium-exchanged reduced pore zorite (Ba-RPZ) and zeolite 4A, *Ind. Eng. Chem. Res.*, 2021, **60**, 10777–10790.

57 Z. Bao, S. Alnemrat, L. Yu, I. Vasiliev, Q. Ren, X. Lu and S. Deng, Adsorption of ethane, ethylene, propane, and propylene on a magnesium-based metal–organic framework, *Langmuir*, 2011, **27**, 13554–13562.